Seismic modeling for P-P and P-SV AVO analysis

Taiwen Chen and Donald C. Lawton

ABSTRACT

Seismic physical and numerical modeling experiments were undertaken in order to compare amplitude versus offset (AVO) responses for P-P and P-SV data collected over simple 2- and 3-layer models. Generally, the physical modeling and numerical modeling results agree rather well. It is clear that increasing the acoustic impedance difference between the overlying and underlying layers increases P-wave reflection amplitudes for the top of the second layer, and decrease the P-wave reflection amplitude for the bottom of the second layer. When the Poisson's ratio of the underlying medium is the same as that of the overlying medium, the P-wave amplitude decreases with increasing offset for both the top and the bottom of the second layer. For the converted wave, it seems that increasing the shear wave velocity for the underlying medium increases the P-SV reflection amplitude for the top of the second layer, and decreases it for the bottom. Besides, this study shows that there is an interesting possibility for recording P-P reflections with a radial-component receiver in areas with a high-velocity surface layer.Current modeling experiments are derived at examining the effect of a high-velocity surface layer on the AVO response of deeper reflectors.

INTRODUCTION

Previous work shows that AVO may be an effective way to distinguish between two kinds of bright spots on conventional stack sections: gas-related and non-gas-related (Ostrander, 1984). Recent work suggests that AVO analysis and inversion might be an effective way to extract rock properties (Smith, et al., 1987; Stewart, 1990). This study provides a comparative AVO analysis for both P-P and P-SV reflection seismic data, using both physical and numerical modeling.

Since 1983, considerable attention has been paid to the problem of seismic data acquisition in areas with a high-velocity surface layer. Seismic data quality is usually degraded by the high-velocity layer (e.g., carbonate, salt, volcanics, anhydride and permafrost). There are some suggested solutions to the problem, such as converted-wave approach (Purnell et al., 1990; Pritchett, 1991) and shear-wave approach (Fix et al., 1983; Danbom and Domenico, 1987). Purnell et al. (1990) and Pritchett (1991) suggested that better energy transmission between the S mode in the high-velocity layer and the P mode elsewhere could be observed. Fix et al. (1983) showed some successful examples of using shear-wave to get interpretable reflection data. This report includes P-P and P-SV physical and numerical studies for a high-velocity surface layer model.

MODEL CONSTRUCTION

Six physical models were set up for AVO analysis. Materials, such as parawax, plaster of Paris, plexiglass, and aluminum, were chosen for these models. These six models were subdivided into two groups in terms of the acoustic impedance difference between the overlying layer and the underlying layer. Group 1 has the positive acoustic impedance difference, which usually indicates that the P-wave velocity for the second layer is greater than that of the first one. Group 2 has the negative acoustic impedance difference. The high-velocity surface layer model is in the second group.

Models with positive acoustic impedance difference

This group includes three models. Model 1 is parawax over plexiglass, and physical parameters for model 1 are listed in Table 1. The change in P-wave velocity between parawax and plexiglass is not large, and Poisson's ratio of parawax (0.40) is bigger than that of plexiglass (0.33).

Table 1: Materials and their physical parameters used in model 1

Compound	Thickness (actual, cm)	Thickness (scaled, m)	V_p (m/s)	V_s (m/s)	σ	ρ (g/cm^3)
Parawax	4.902	490.2	2133	874	0.40	0.90
Plexiglass	1.237	123.7	2740	1380	0.33	1.15

Model 2 is parawax over aluminum, and model 3 is plexiglass over aluminum. The physical parameters are listed in Table 2 and Table 3, respectively. Aluminum has a very high P-wave velocity, hence a large acoustic impedance boundary exists between parawax and aluminum, also between plexiglass and aluminum. This is similar to the large impedance boundary between the Mississippian carbonates and overlying Cretaceous sediments in southern Alberta (Lawton, et al., 1989).

Table 2: Materials and their physical parameters used in model 2

Compound	Thickness (actual, cm)	Thickness (scaled, m)	V_p (m/s)	V_s (m/s)	σ	ρ (g/cm^3)
Parawax	4.902	490.2	2133	874	0.40	0.90
Aluminum	1.307	130.7	6004	3029	0.33	2.64

Table 3: Materials and their physical parameters used in model 3

Compound	Thickness (actual, cm)	Thickness (scaled, m)	V_p (m/s)	V_s (m/s)	σ	ρ (g/cm^3)
Plexiglass	14.23	1423	2740	1380	0.33	1.15
Aluminum	5.00	500	6004	3029	0.33	2.64

Models with negative acoustic impedance difference

This group includes three models. Model 4 is parawax over plaster of Paris; Table 4 lists physical parameters of this model. Plaster of Paris has a relative low Poisson's ratio (0.19), and it was used to model gas-bearing sands. Parawax has a high Poisson's ratio (0.4), and it was used as the 'overlying rock' (e.g., shale) for the 'gas sand'. The contrast in Poisson's ratio for this model is similar to that discussed by Ostrander (1984).

Table 4: Materials and their physical parameters used in model 4

Compound	Thickness (actual, cm)	Thickness (scaled, m)	V_p (m/s)	V_s (m/s)	σ	ρ (g/cm^3)
Parawax	4.902	490.2	2133	874	0.40	0.90
Plaster of Paris	1.540	154.0	1825	1130	0.19	0.92

Model 5 is plexiglass over air, Table 5 lists the physical parameters. Model 6 is aluminum over plexiglass; Table 6 lists physical parameters. In model 6, the aluminum layer represents the high-velocity surface layer, although a rather extreme case. The underlying layer has a P-wave velocity around 2750 m/s, with a thickness of about 1500 m, representing a normal sedimentary sequence.

Table 5: Materials and their physical parameters used in model 5

Compound	Thickness (actual, cm)	Thickness (scaled, m)	V_p (m/s)	V_s (m/s)	σ	ρ (g/cm^3)
Plexiglass	14.23	1423	2740	1380	0.33	1.15
Air	5.00	500	340	0	0.50	0.00

Table 6: Materials and their physical parameters used in model 6

Compound	Thickness (actual, cm)	Thickness (scaled, m)	V_p (m/s)	V_s (m/s)	σ	ρ (g/cm^3)
Aluminum	1.32	132	6004	3029	0.33	2.64
Plexiglass	14.23	1423	2740	1380	0.33	1.15

MODELING

Elastic modeling

For all six models, both P-P and P-SV surveys were undertaken. Cylindrical transducers were used as the source and the receiver, which were first located in the middle part of the model. Data were collected in a CMP format by moving the source and receiver in opposite directions (Figure 1), starting from a near offset of 200 m (scaled) for models

1, 2, and 4, and 250 m (scaled) for the remaining models. Table 7 summarizes the geometry of the survey.

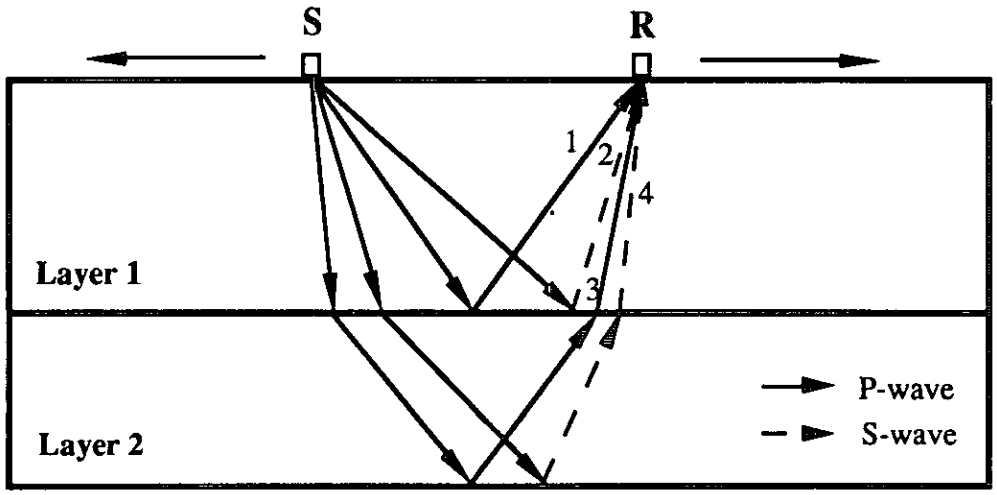

FIG.1. P-P and P-SV survey over the model

S: source; R: receiver; 1: PP; 2: PS; 3: PPPP; 4: PPSS

Table 7: Scaled acquisition and recording parameters for the model

Source:	transducer
Receiver:	transducer
Receivers per shot:	50 (or 60)
Group interval:	50 m
Data format:	SEGY
Record length:	3000 ms
Sample interval:	1 ms

In Figure 1 and the following discussion, PP refers to the incident P-wave was reflected back at the top of second layer in P mode, and PS refers to the wave was reflected in S mode. PPPP refers to the incident P-wave was transmitted to the second layer in P mode, reflected back at the bottom of the second layer in P mode. Then the reflected P-wave transmitted through the boundary between the first and the second layer in P mode. PPSS refers to the incident P-wave was transmitted to the second layer in P mode, reflected back at the bottom of the second layer in S mode. Then the reflected S-wave was transmitted through the boundary between the first and the second layer in S mode.

Numerical modeling

Numerical modeling was also undertaken for comparison with the physical modeling results. Reflection coefficients for both P-P and P-SV were calculated using Zoeppritz equations. All numerical modeling data were computed using in-house software developed by D.C. Lawton and E.S. Krebes. Ricker wavelets (35 Hz) were chosen for the synthetic data since this approximately matched the bandwidth of most of the physical modeling data (after scaling). For all numerical models, geometrical spreading and

transmission losses were included, but inelastic attenuation was not. This is the main difference between the physical modeling and the numerical modeling.

RESULTS AND DISCUSSION

Figures 2, 3, and 5 show results of modeling with the parawax as the surface layer. These data are very noisy, a result interpreted to be caused by scattering from small bubbles within the wax, and inconsistent coupling between the transducers and the slightly, irregular, soft surface of the wax. The low frequency of all the data in Figures 2, 3 and 5 indicates that the seismic energy is also highly attenuated in the wax layer.

Comparison between the results of physical and numerical modeling for these models shows consistency between traveltime of identified events, but physical data are generally too noisy to be able to make definitive statements about phase and amplitude variations with source-receiver offset. However, model 2 (Figure 3) shows cross-over of reflections from the base and top of the aluminum layer. Also, the physical model data for the P-P case (Figure 3a) shows a polarity reversal (at the far offset) for the PP refection from the top of the aluminum layer.

In Figure 5a, the Poisson's ratio for the second layer (plaster of Paris) is smaller than that of the first layer (plexiglass), and the reflection coefficient at the normal incidence is negative. Therefore, the PP amplitude increases with increasing offset, which can be observed on both physical and numerical modeling for small offsets. From middle to far offset, the PP amplitude decreases with increasing offset, this is due to the geometrical spreading and transmission losses applied to both physical and numerical modeling, and also due to the attenuation for the physical modeling.

The results of numerical P-P modeling in Figures 2a, 3a and 5a infer that increasing the acoustic impedance difference between the first and second layer will increase the PP reflection amplitude, and decrease the PPPP reflection amplitude. Results of both physical and numerical modeling in Figures 2b, 3b and 5b suggests that increasing the shear wave velocity for the underlying medium increase the reflection amplitude for PS case, and a decrease for PPSS.

The second set of models, using plexiglass as the surface layer, generally provide better data quality than those models discussed above (parawax as the surface layer). In Figure 4 and 6 (models 3 and 5, respectively), there is an excellent match between the traveltimes of events in the numerical and physical data, for both P-P and P-SV cases. However, the AVO effects are not as well matched, possibly due to attenuation in the physical model data which was not incorporated into the numerical modeling.

Figure 7 shows results of P-P and P-SV modeling for the case of the high-velocity surface layer (model 6) (exponential gain was used for Figure 7). Reflections from the base of layer 2 (plexiglass) are severely degraded by the presence of the high-velocity surface layer. The reverberation of energy within this aluminum layer is very evident in records. The rapid decline in the PPPP event amplitude with increasing offset (Figure 7a) is a result of severe refraction at the aluminum/plexiglass boundary. In this case, the interesting possibility exists for recording P-P reflection with the radial-component receiver. Figure 7b shows that PPPP event are indeed recorded in the P-SV data set for all source-receiver offsets. Comparing Figure 6b and 7b, one may conclude that P-P reflections perhaps can be recorded with radial-component receivers in areas with a high-velocity surface layer.

In Figure 7b, an event around 2 seconds for offsets around 200 m can be observed. This event can also be seen in Figure 7a. This may be the reflected energy with the combination of P and S mode in its travelpath. This would infer that reflected seismic energy with the combination of P mode and S mode may be used for seismic exploration in areas with a high-velocity surface layer.

In Figures 4a and 7a, The Poisson's ratio of the second layer is equal to that of the first layer. For both the positive normal incidence reflection (plexiglass over aluminum) and the negative normal incidence reflection (aluminum over plexiglass) cases, PP and PPPP amplitude decreases with increasing offset.

CONCLUSIONS AND FUTURE WORK

Four conclusions can be drawn from this study:

(1): Increasing the acoustic impedance difference between the overlying and underlying layer will increase the PP reflection amplitude and decrease the PPPP reflection amplitude. Increasing the shear wave velocity for the underlying medium would increase the reflection amplitude for PS case, decrease for PPSS.

(2): When the Poisson's ratio of the underlying medium is the same as that of the overlying medium, the PP and PPPP amplitude decreases with increasing offset.

(3): Parawax is not a suitable modeling material for quantitative AVO analysis.

(4): There is an interesting possibility for recording P-P reflection with the radial-component receiver in areas with a high-velocity surface layer. Also, the result from the high-velocity surface layer model infers that the reflected seismic energy with the combination of P mode and S mode might be useful for seismic exploration for deeper reflector in areas with the high velocity surface layer.

As we mentioned earlier, P-wave velocity of aluminum may be too large compared to the P-wave velocity of the real high-velocity surface layer. For the further physical modeling AVO analysis, we will choose a more suitable material with a lower P-wave velocity (around 4000 m/s). Also, aluminum is relatively homogeneous. Inhomogeneous and anisotropic material such as phenolic will also be used in our further modeling study of high velocity surface layers.

ACKNOWLEDGEMENT

We would like to thank sponsors of the CREWES project for the continuous support. Mr Eric Gallant gave us the technical and lab assistance. The first author would also like to thank CREWES project for the financial support as the graduate student research assistantship.

REFERENCES

Danbom, S.H., and Domenico, S.N., 1987, Shear-wave exploration: SEG.

Fix, J.E., Robertson, J.D., and Pritchett, W.C., 1983, Shear-wave reflections in three west Texas basins with high-velocity surface rocks: 53rd Ann. Internat. Mtg., Soc. Expl. Geophy., Expanded Abstracts, 414-416.

Lawton, D.C., Cheadle, S.P., Gallant, E.V., and Bertram, M.B., 1989, Physical seismic modeling of sand-filled channels: University of Calgary, CREWES Project report, v. 1, 342-344.

Ostrander, W. J., 1984, Plane-wave reflection coefficients for gas sands at normal angles of incidence: Geophysics, 49, 1637-1648.

Pritchett, W.C., 1990, Acquiring better seismic data: Chapman and Hall.

_____, 1990, Problems and answers in recording reflection from beneath Karst or Volcanic surfaces: 60th Ann. Internat. Mtg., Soc. Expl. Geophy., Expanded Abstracts, 922-925.

Purnell, G.W., McDonald, J.A., Sekharan, K.K., and Gardner, G.H.F., 1990, Imaging beneath a high-velocity layer using converted waves: 60th Ann. Internat. Mtg., Soc. Expl. Geophy., Expanded Abstracts, 752-755.

Smith, G.C., and Gidlow, P.M., 1987, Weighted stacking for rock property estimation and detection of gas: Geophys. Prosp., 35, 993-1014.

Stewart, R.R., 1990, Joint P and P-SV inversion: University of Calgary, CREWES Project report, v.2, 112-115.

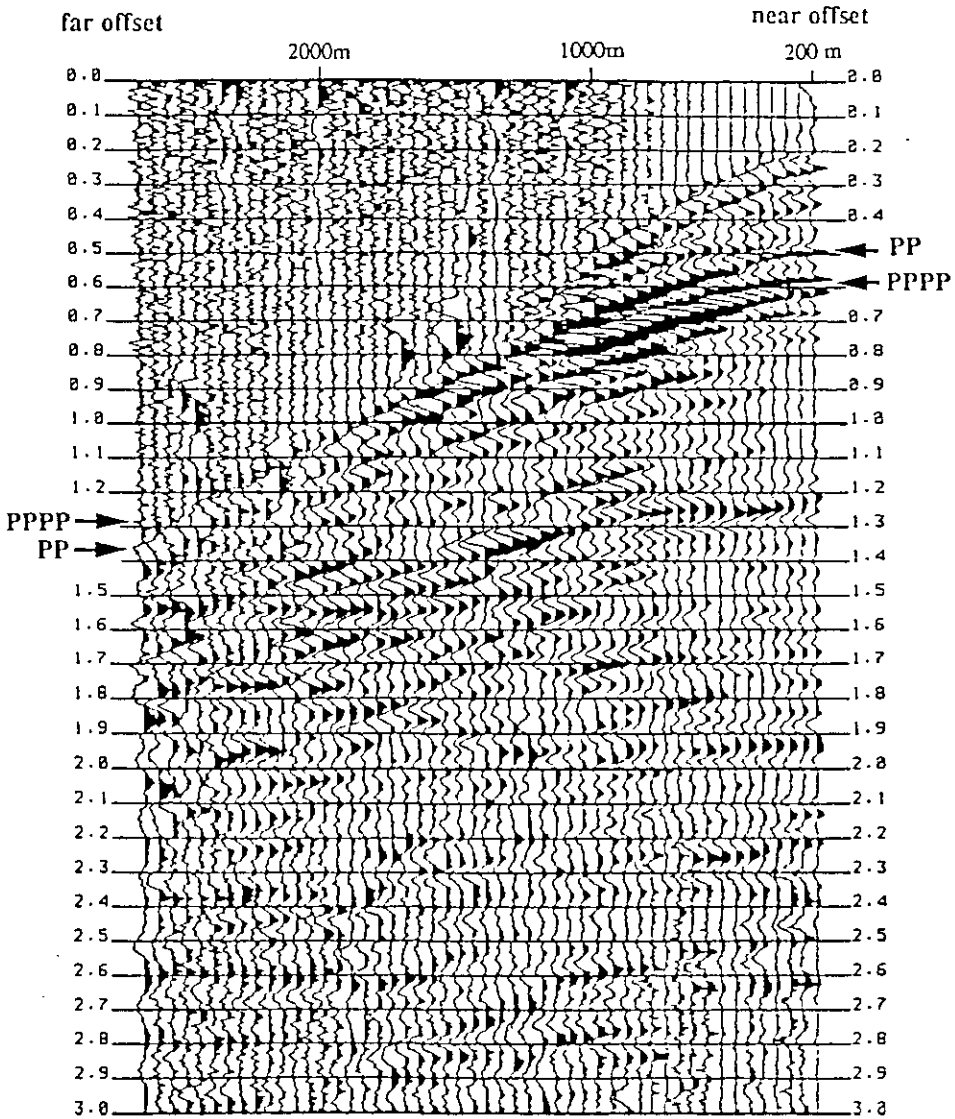

Physical seismic data

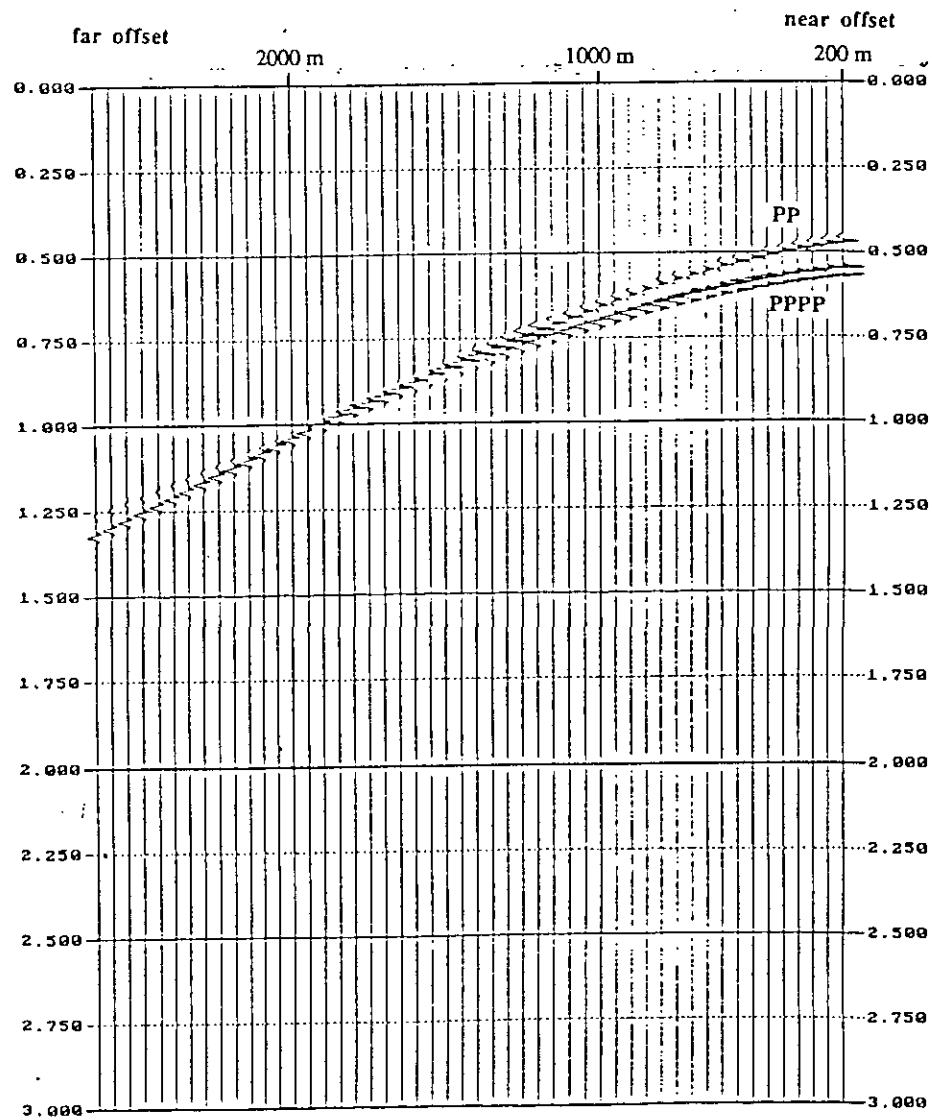

Numerical seismic data

FIG. 2a. P-P seismic data, parawax over plexiglass (model 1).

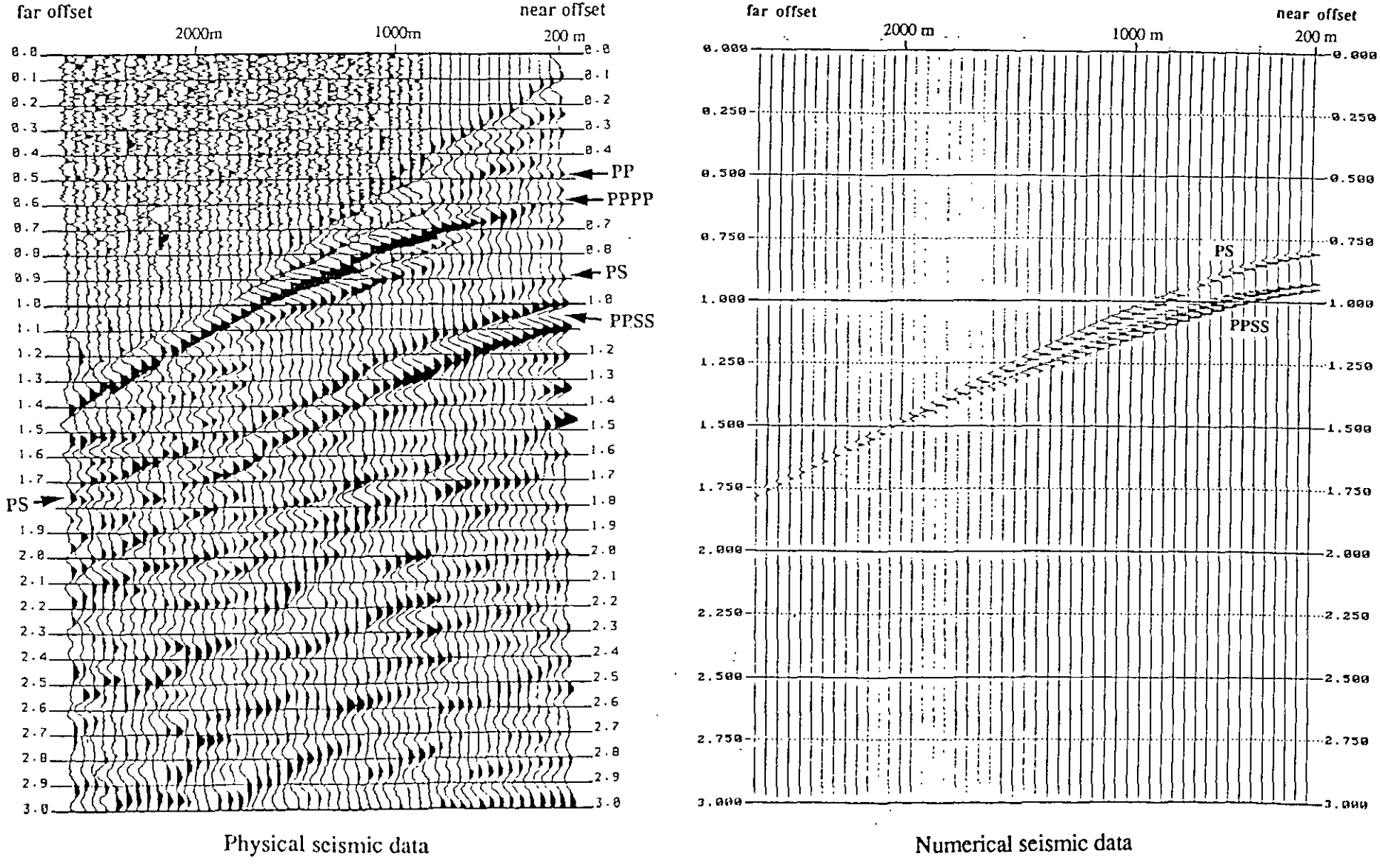

Physical seismic data

Numerical seismic data

FIG. 2b. P-SV seismic data, parawax over plexiglass (model 1).

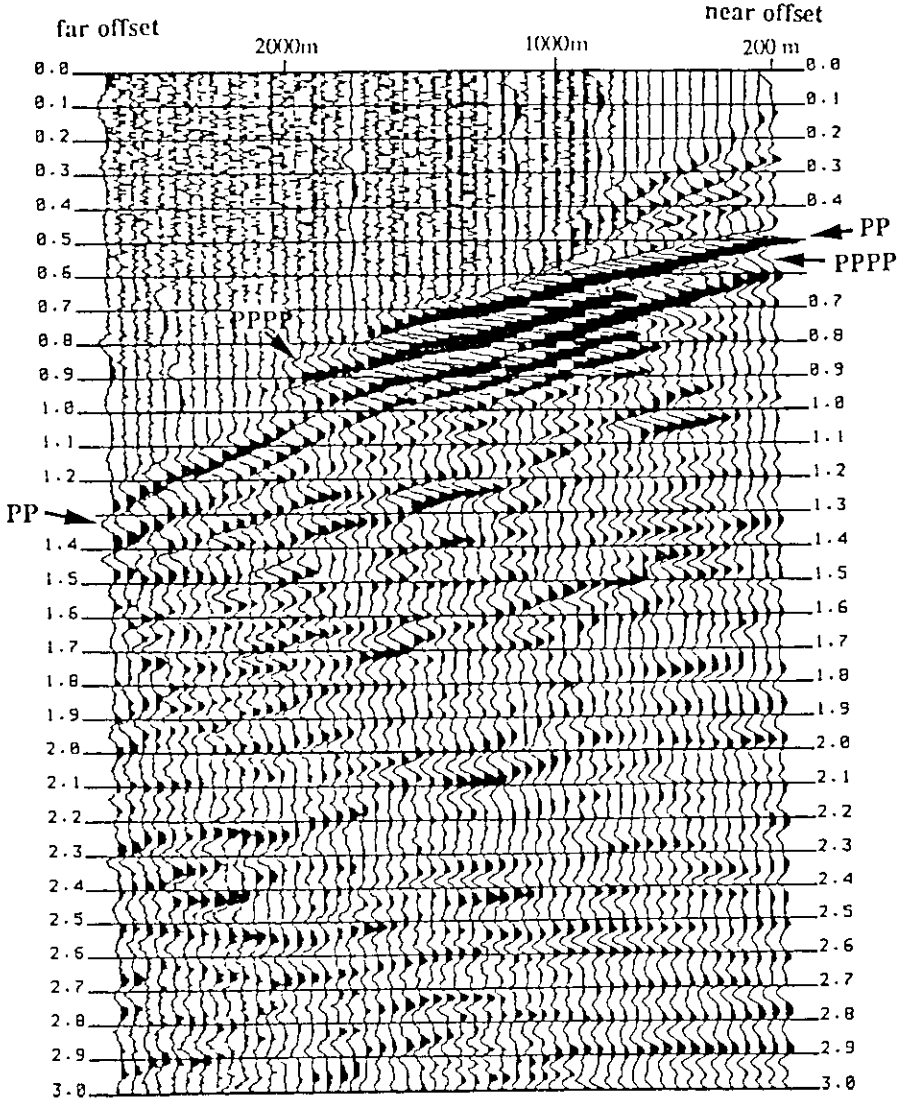

Physical seismic data

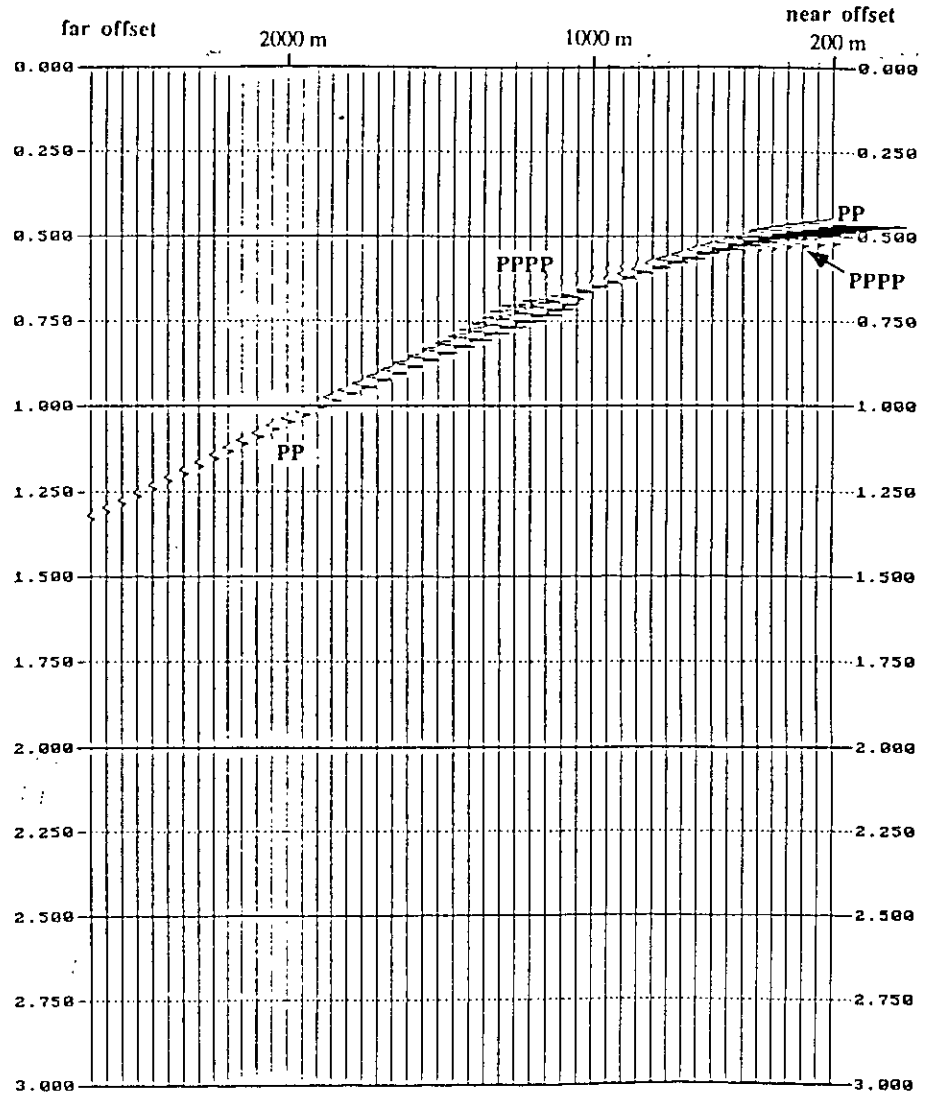

Numerical seismic data

FIG. 3a. P-P seismic data, parawax over aluminum (model 2).

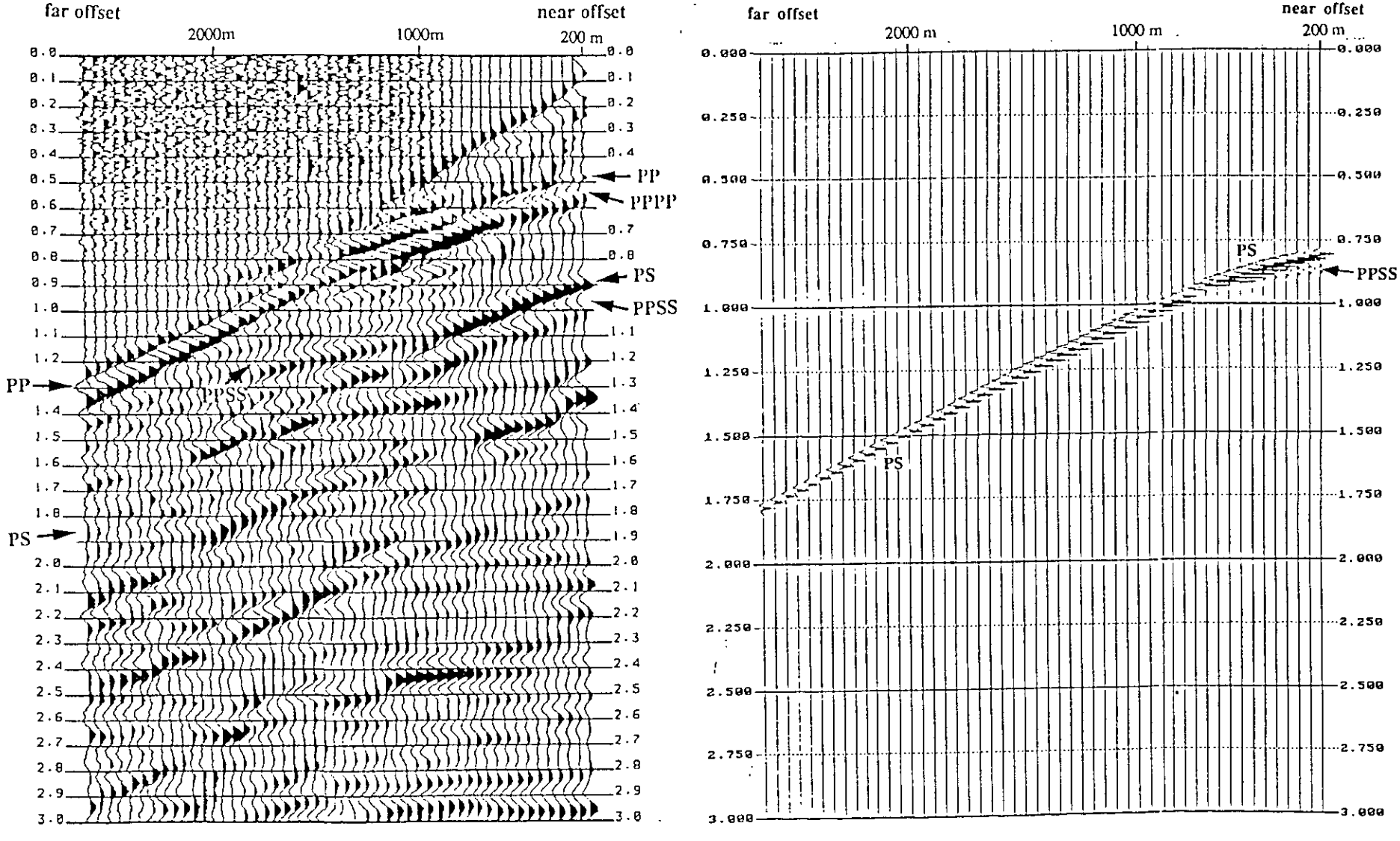

Physical seismic data

Numerical seismic data

FIG. 3b. P-SV seismic data, parawax over aluminum (model 2).

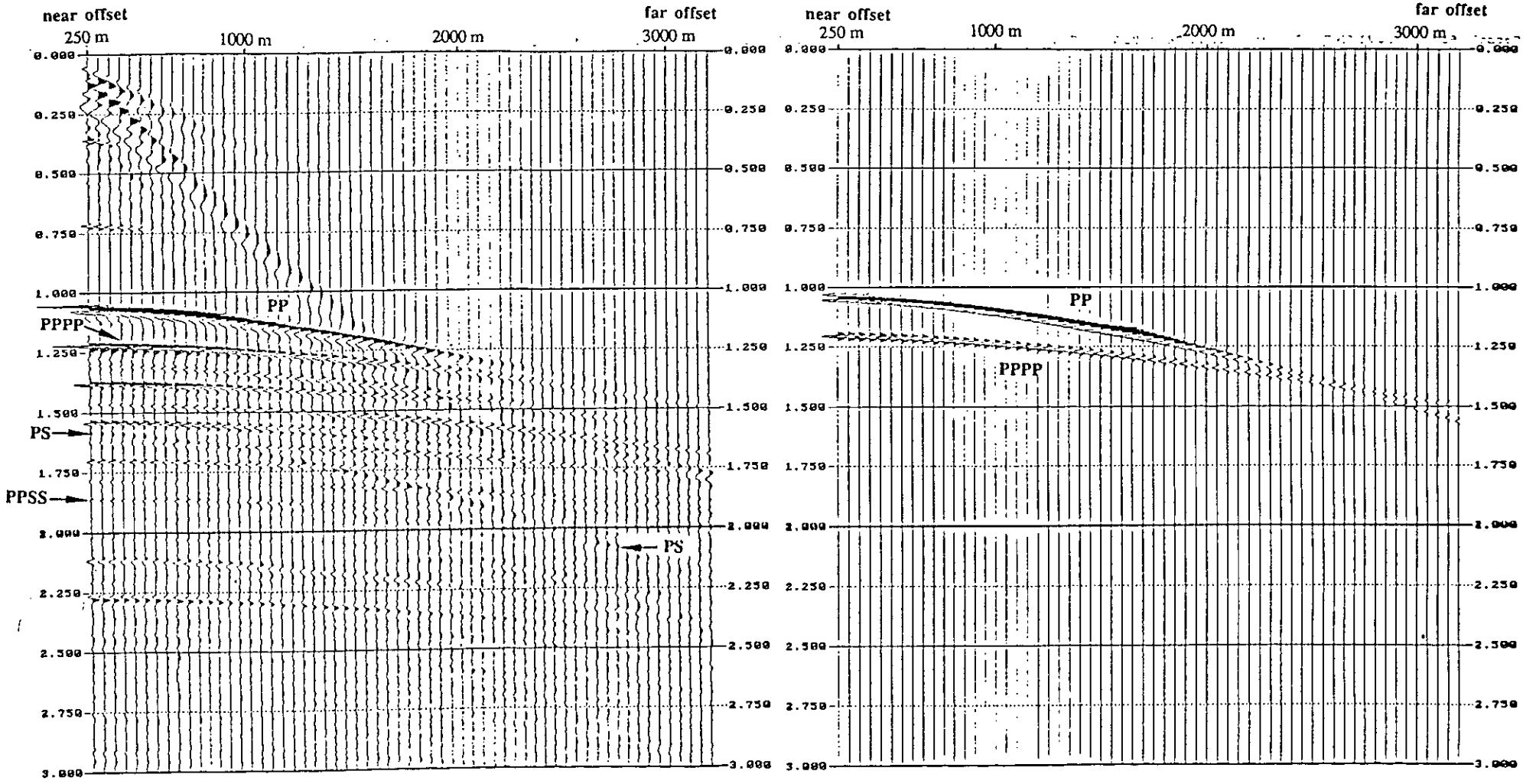

Physical seismic data

Numerical seismic data

FIG. 4a. P-P seismic data, plexiglass over aluminum (model 3).

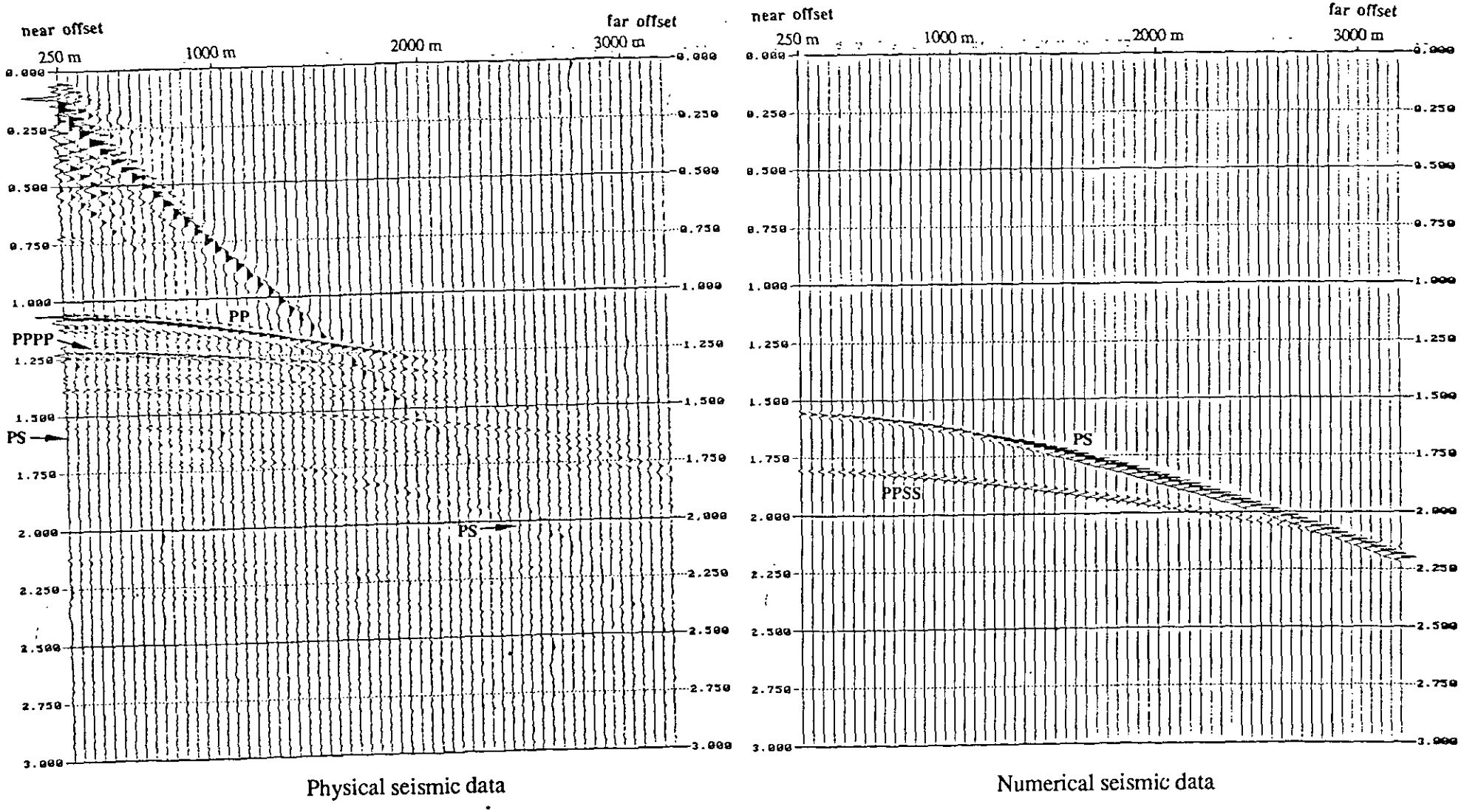

Physical seismic data

Numerical seismic data

FIG. 4b. P-SV seismic data, plexiglass over aluminum (model 3).

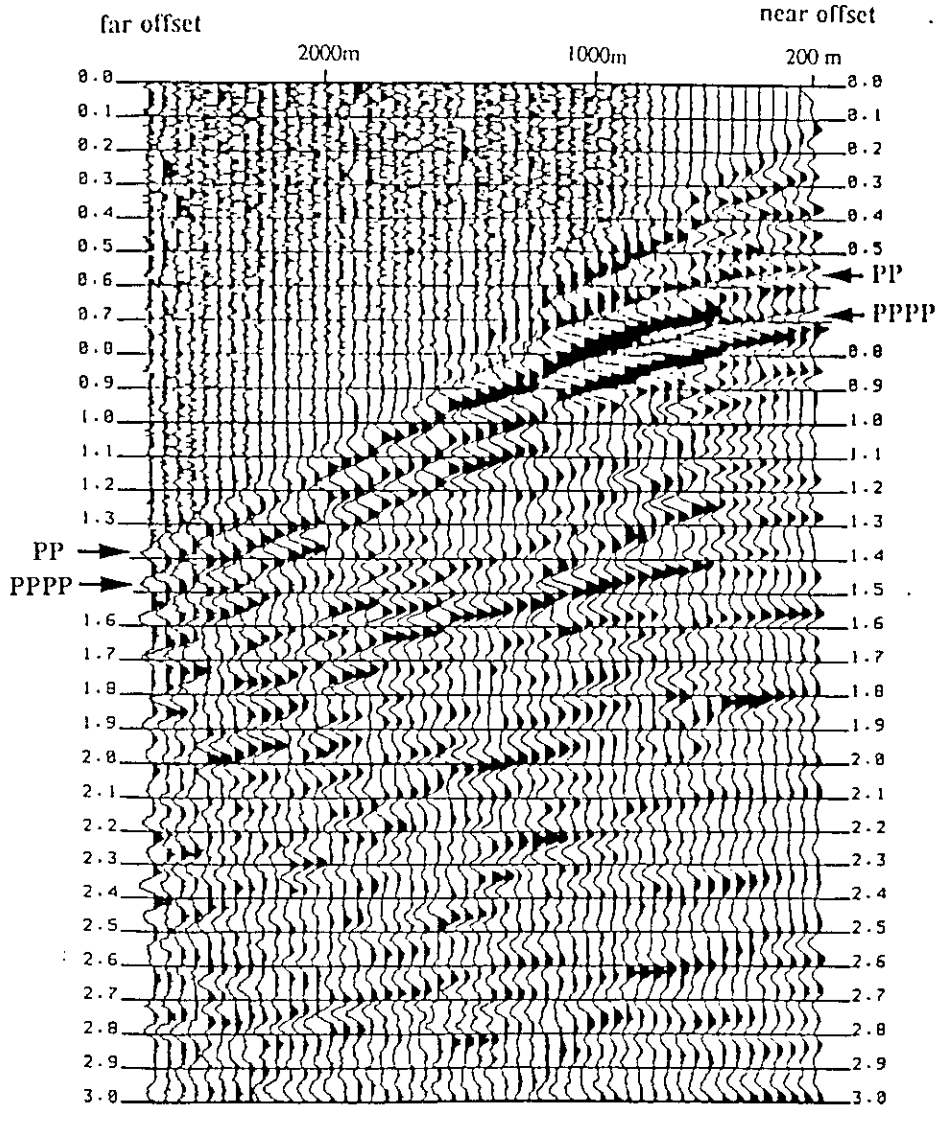

Physical seismic data

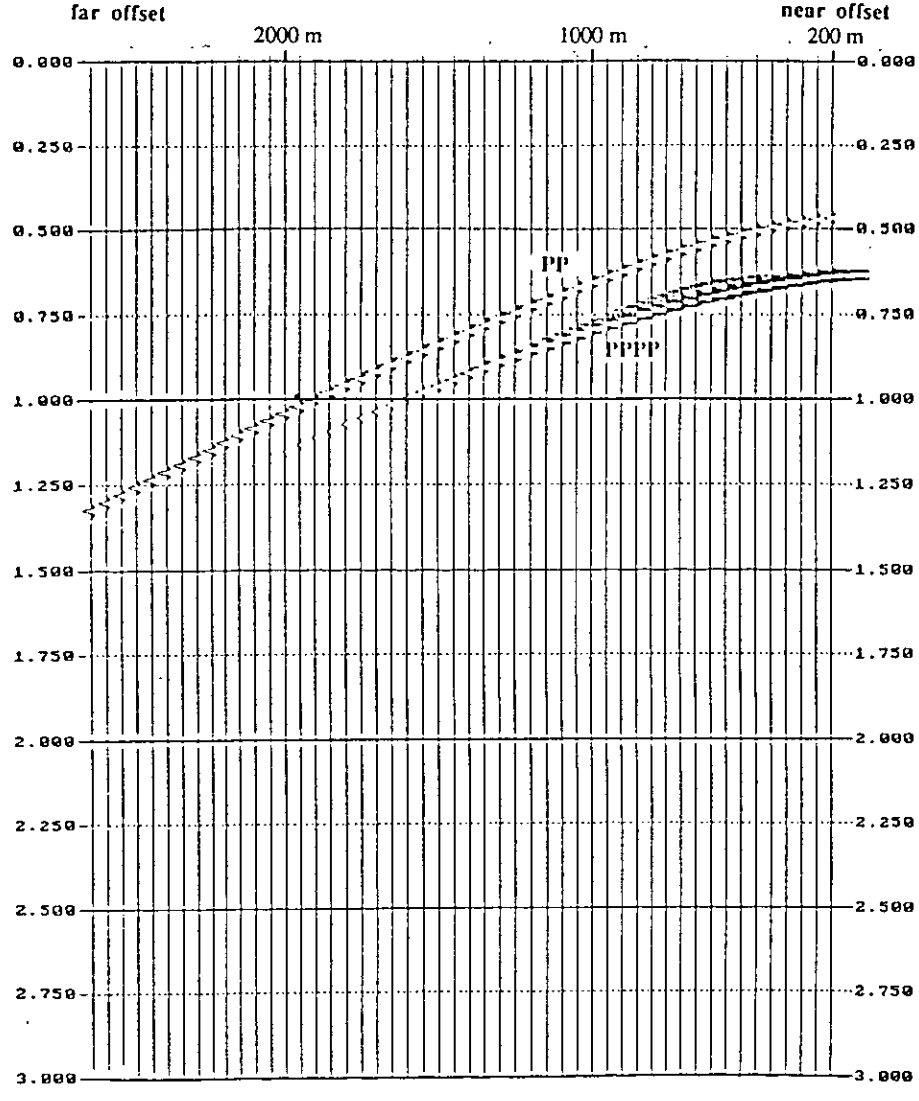

Numerical seismic data

FIG. 5a. P-P seismic data, parawax over plaster of Paris (model 4).

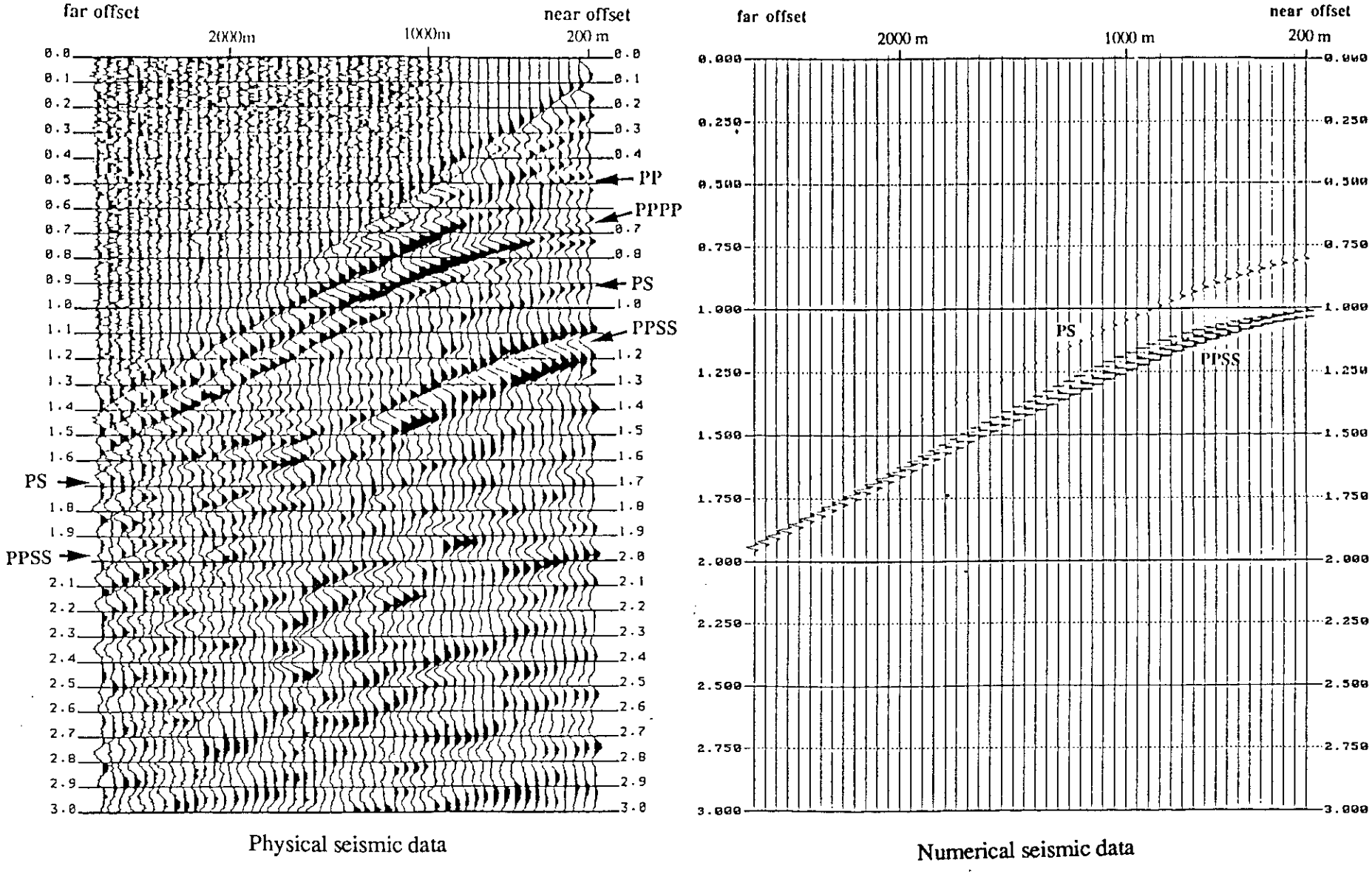

FIG. 5b. P-SV seismic data, parawax over plaster of Paris (model 4).

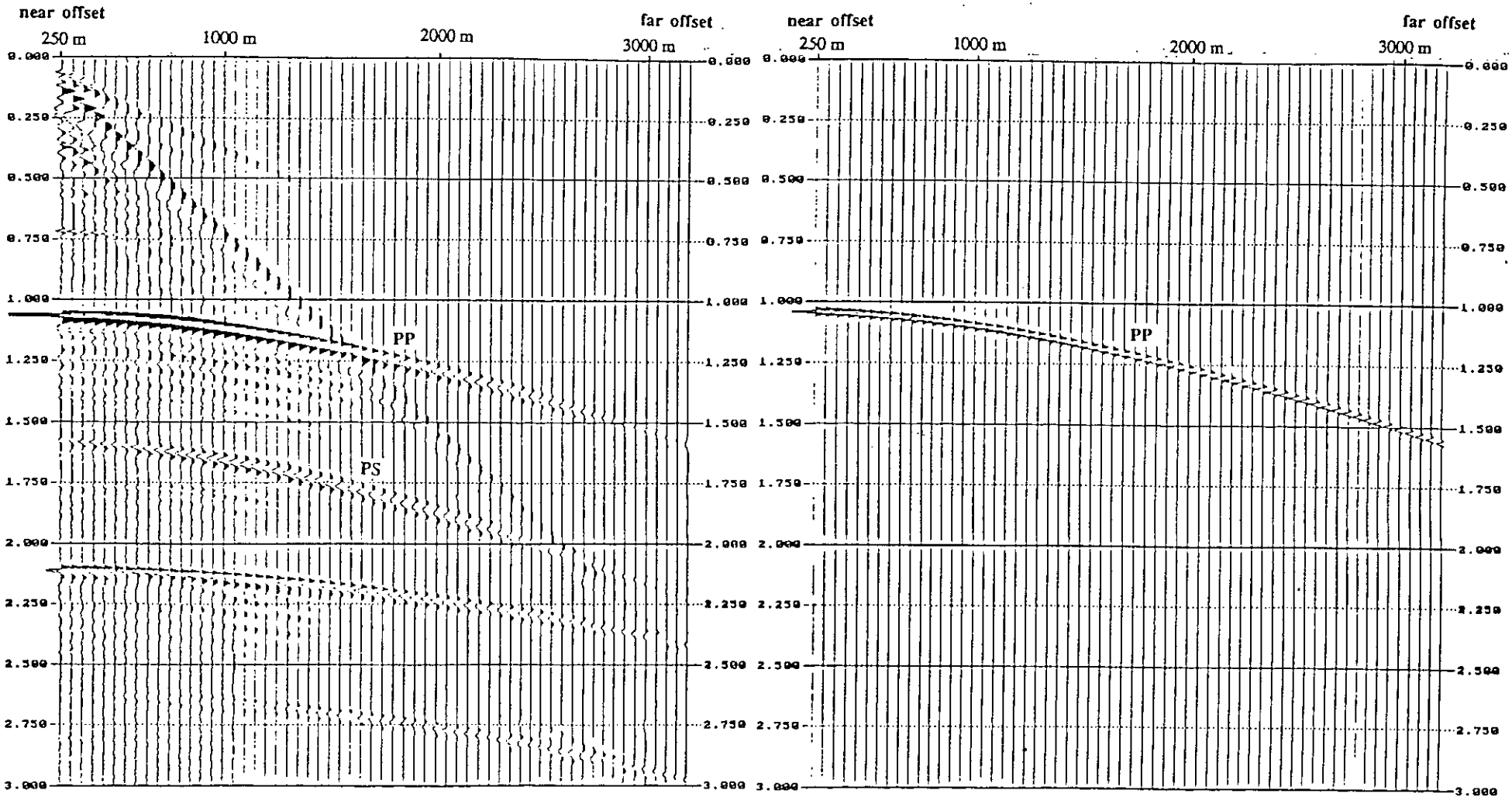

Physical seismic data

Numerical seismic data

FIG. 6a. P-P seismic data, plexiglass over air (model 5).

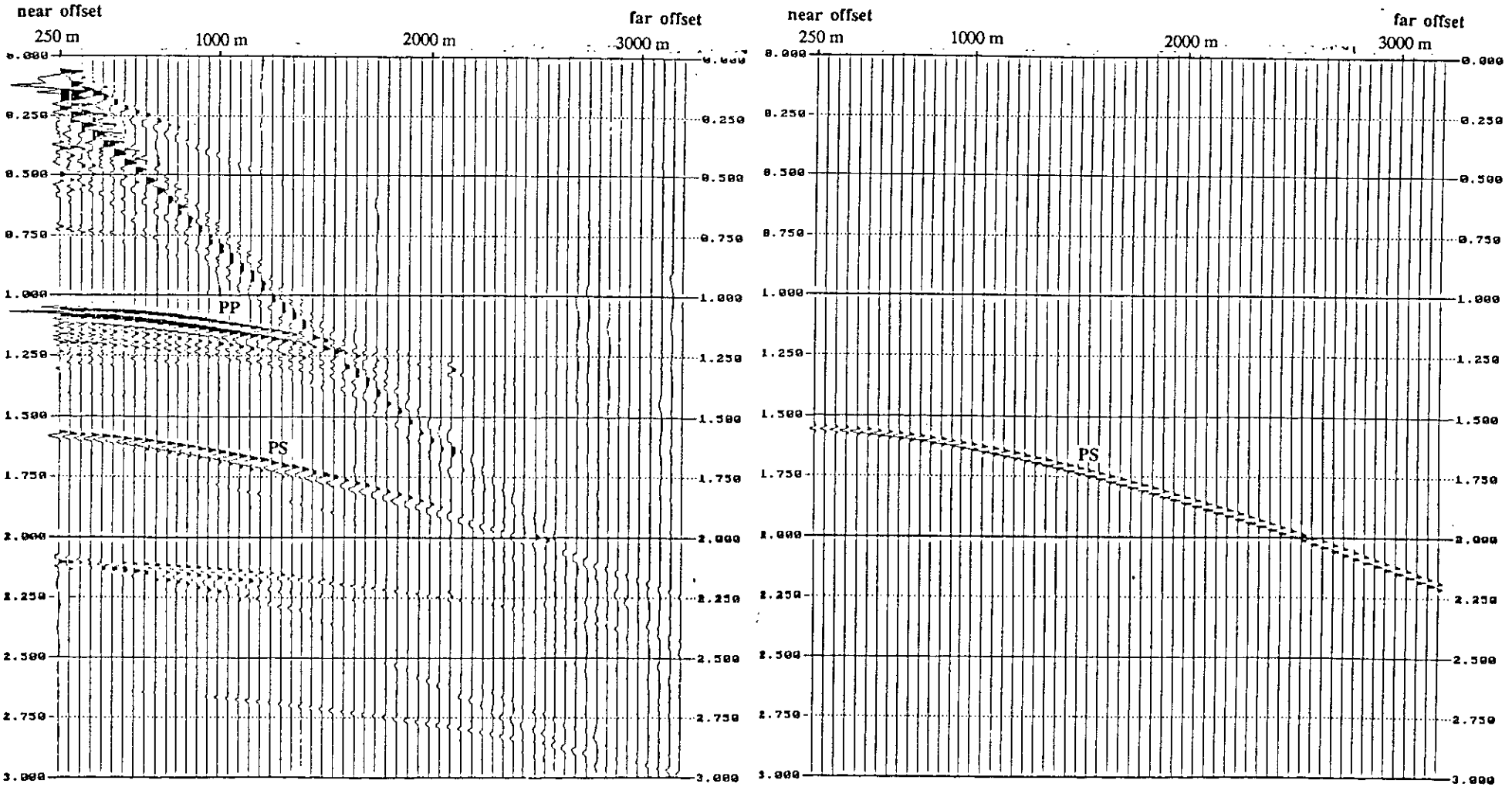

Physical seismic data

Numerical seismic data

FIG. 6b. P-SV seismic data, plexiglass over air (model 5).

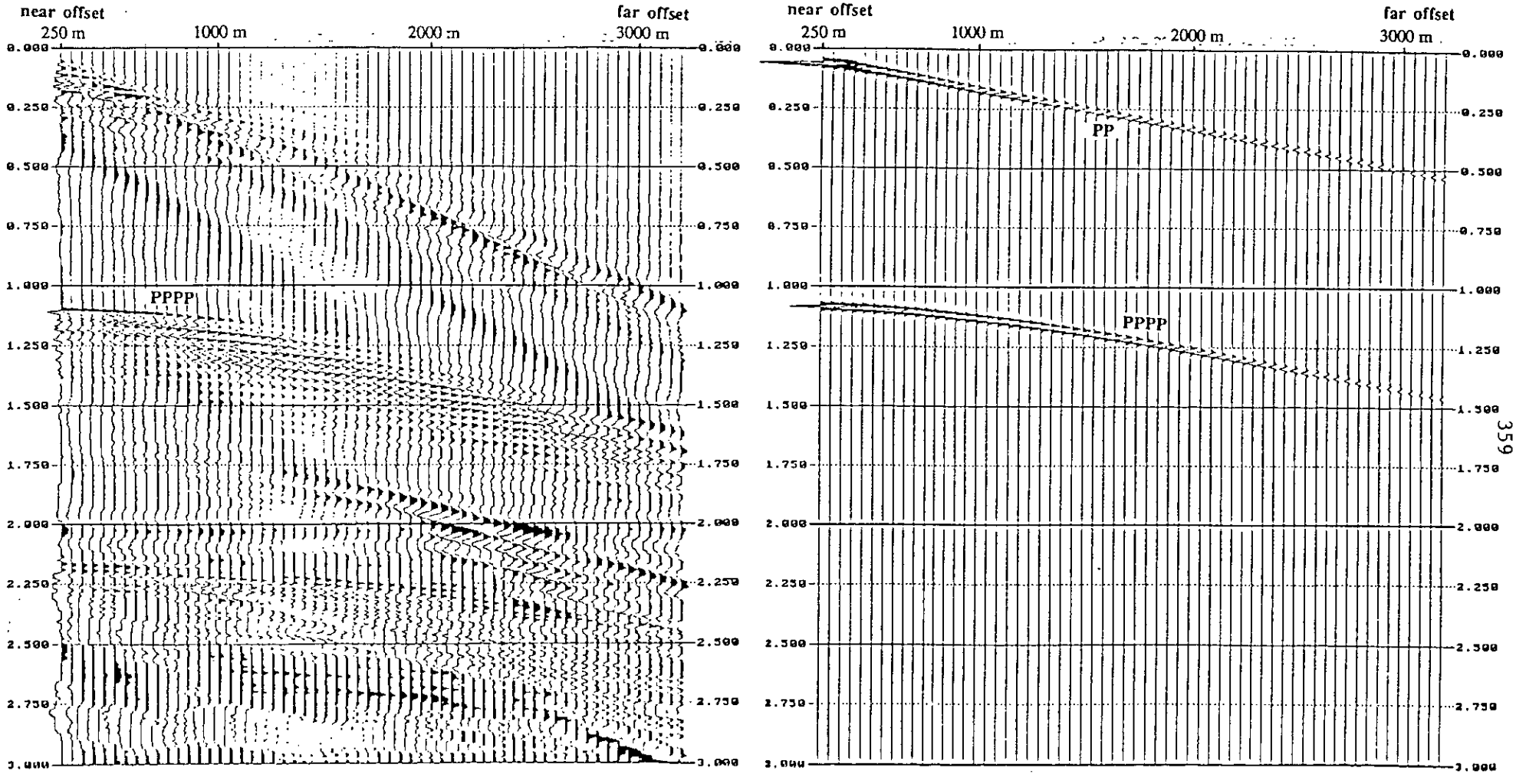

Physical seismic data

Numerical seismic data

FIG. 7a. P-P seismic data, aluminum over plexiglass (model 6).

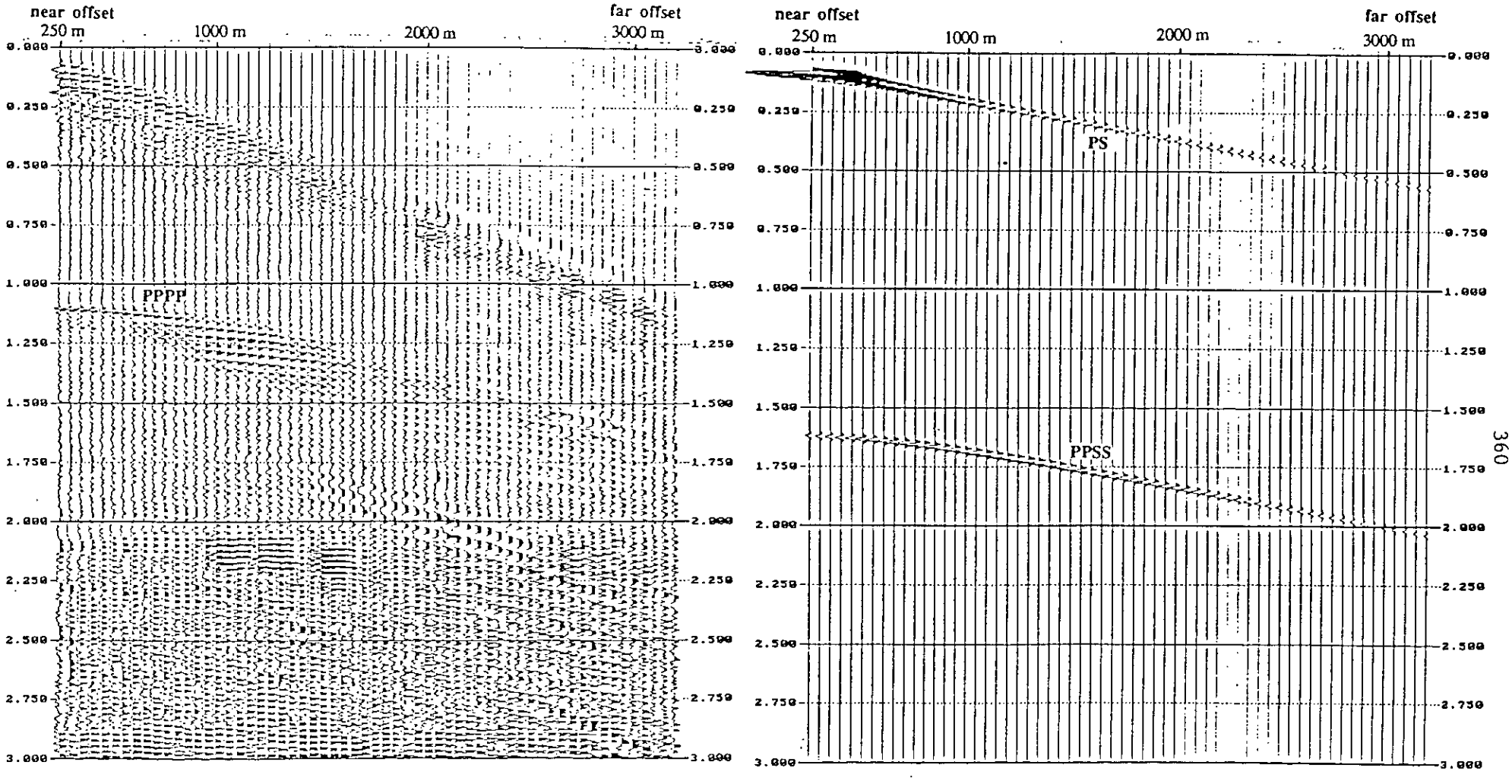

FIG. 7b. P-SV seismic data, aluminum over plexiglass (model 6).